

THE ORIGIN OF R-PROCESS ELEMENTS IN THE MILKY WAY

BENOIT CÔTÉ^{1,7,8}, CHRIS L. FRYER^{2,7,8}, KRZYSZTOF BELCZYNSKI³, OLEG KOROBKIN^{2,7}, MARTYNA CHRUŚLIŃSKA⁴, NICOLE VASSH⁵, MATTHEW R. MUMPOWER^{2,6,7}, JONAS LIPPUNER^{2,7}, TREVOR M. SPROUSE⁵, REBECCA SURMAN^{5,7}, RYAN WOLLAEGER²

Draft version December 14, 2024

ABSTRACT

Some of the heavy elements, such as gold and europium (Eu), are almost exclusively formed by the rapid neutron capture process (r-process). However, it is still unclear which astrophysical site between core-collapse supernovae and neutron star - neutron star (NS-NS) mergers produced most of the r-process elements in the universe. Galactic chemical evolution (GCE) models can test these scenarios by quantifying the frequency and yields required to reproduce the amount of Eu observed in galaxies. Although NS-NS mergers have become popular candidates, their required frequency (or rate) needs to be consistent with that obtained from gravitational wave measurements. Here we address the first NS-NS merger detected by LIGO/Virgo (GW170817) and its associated Gamma-ray burst and analyze their implication on the origin of r-process elements. Among other elements, we find that this event has produced between 15 and 70 Earth masses of gold. The range of NS-NS merger rate densities of $320 - 4740 \text{ Gpc}^{-3} \text{ yr}^{-1}$ provided by LIGO/Virgo is remarkably consistent with the range required by GCE to explain the Eu abundances in the Milky Way with NS-NS mergers, assuming a typical r-process abundance pattern for the ejecta. When using theoretical calculations to derive Eu yields, constraining the role of NS-NS mergers becomes more challenging because of nuclear astrophysics uncertainties. This is the first study that directly combines nuclear physics uncertainties with GCE calculations. If GW170817 is a representative event, NS-NS mergers can produce Eu in sufficient amount and are likely to be the main r-process site.

Subject headings: Binaries: close — Stars: abundances — processes: nucleosynthesis — Physical Data and Processes: gravitational waves

1. INTRODUCTION

Core-collapse supernovae (CC SNe) and neutron star - neutron star (NS-NS) mergers are the two leading candidates for producing most of the rapid neutron capture process (r-process) elements in the universe (e.g., Arnould et al. 2007; Matteucci et al. 2014; Cescutti et al. 2015; Wehmeyer et al. 2015). NS-NS mergers, originally proposed by Lattimer & Schramm (1974), recently gained popularity because the high neutron fraction allows robust production of the 2nd and 3rd r-process peaks (e.g., Korobkin et al. 2012; Thielemann et al. 2017, but see Nishimura et al. 2015). If NS-NS mergers are indeed more likely to produce the full r-process, the challenge is now to determine whether the rate of NS-NS mergers is high enough to explain the r-process enrichment observed in the Milky Way and other galaxies.

In Côté et al. (2017a, C17a), we derived the rate of

NS-NS mergers required in galactic chemical evolution (GCE) studies in order to match the amount of europium (Eu) observed in the Milky Way. Eu in the solar system is almost entirely made by the r-process (Burris et al. 2000) and is therefore used as a tracer. We found that the required rates can be consistent with the upper limits provided by Advanced LIGO during their first observing run (Abbott et al. 2016).

In this Letter, we update our analysis to address the first NS-NS merger ever detected via gravitational waves (GW170817, Abbott et al. 2017), which provides new estimates for the NS-NS merger rate density in the nearby universe. This merger manifested itself across the entire electromagnetic spectrum from radio through gamma-rays, providing additional constraints on the location, distance, and the ejecta mass and composition (Cowperthwaite et al. 2017; Tanvir et al. 2017; Troja et al. 2017; Evans et al. 2017).

This paper is organized as follows. We present in Section 2 the NS-NS merger yields derived from the multi-wavelength observations of GW170817. In Section 3, we tie our GCE and population synthesis predictions with the latest LIGO/Virgo rate and yield measurements. We discuss the implication of this new detection in Section 4, and conclude in Section 5.

2. MERGER YIELDS

The ejecta from NS-NS mergers can be classified into two main categories which are distinguished by the time of ejection: dynamical ejecta, generated at the time of contact, and everything else which emerges after the sin-

¹ Konkoly Observatory, Research Centre for Astronomy and Earth Sciences, Hungarian Academy of Sciences, Konkoly Thege Miklós ut 15-17, H-1121 Budapest, Hungary

² Center for Theoretical Astrophysics, LANL, Los Alamos, NM, 87545, USA

³ Nicolaus Copernicus Astronomical Center, Polish Academy of Sciences, ul. Bartycka 18, 00-716 Warsaw, Poland

⁴ Institute of Mathematics, Astrophysics and Particle Physics, Radboud University Nijmegen, PO box 9010, 6500 GL Nijmegen, the Netherlands

⁵ University of Notre Dame, Notre Dame, Indiana 46556, USA

⁶ Theoretical Division, Los Alamos National Lab, Los Alamos, NM, 87545, USA

⁷ Joint Institute for Nuclear Astrophysics - Center for the Evolution of the Elements, USA

⁸ NuGrid Collaboration, <http://nugridstars.org>

gle object is formed, broadly referred to as “wind” ejecta either from a disk or a hypermassive neutron star (Wollaeger et al. 2017). Estimates of the dynamical ejecta mass in various theoretical models vary from $10^{-4} M_{\odot}$ to $0.1 M_{\odot}$ (see e.g. Hotokezaka et al. 2013, Bovard et al. 2017, Côté et al. 2017a, and Dietrich & Ujevic 2017 for reviews). The dynamical ejecta is expelled so fast that it preserves very low electron fraction ($Y_e < 0.2$, Rosswog 2013), leading to the robust production of the so-called “main” r-process from the 2nd to 3rd r-process peaks (e.g., Figure 3 of Wollaeger et al. 2017). However, general relativistic simulations which include neutrino irradiation predict a broader distribution of Y_e with a tail which extends over 0.3 (e.g. Bovard et al. 2017). A distribution such as this covers the entire r-process range from the 1st peak all the way to the 3rd.

Estimates for the masses in the “wind” category of the ejecta vary from $10^{-4} M_{\odot}$ up to a few $10^{-1} M_{\odot}$ (Just et al. 2015; Côté et al. 2017a). The electron fraction distribution, and hence the composition, of the wind ejecta is also uncertain. However, the general consensus is that the wind ejecta should have a higher electron fraction ($Y_e = 0.2 - 0.5$) than the dynamical ejecta, thus producing isotopes in the range between the 1st and 2nd r-process peaks, or even near the iron peak for particularly high Y_e values (Lippuner & Roberts 2015; Lippuner et al. 2017).

Until now, attempts to detect kilonova were limited to observations of nearby gamma-ray bursts, placing only weak constraints on the ejecta mass and composition. The infrared excess in GRB 130603B (Tanvir et al. 2013) suggested $\sim 0.05 M_{\odot}$ of neutron rich ejecta. But the accompanying bump in X-ray emission points instead to an afterglow flare origin for the infrared excess, arguing for a lower ejecta mass for the neutron rich material. Other studies found $\sim 0.1 M_{\odot}$ in the case of GRB 050714 (Yang et al. 2015) and similarly high mass for GRB 060614 (Jin et al. 2015), which due to the uncertainties could still be treated as strict upper limits on the ejecta mass. Upper limits from GRB 160821B are more strict, suggesting that at least some bursts have less than $0.01 - 0.03 M_{\odot}$ of neutron rich ejecta (Kasliwal et al. 2017).

2.1. Ejecta From GW170817

Fits to the ultraviolet (UV), optical, and infrared data from GW170817 were performed with two-component models based on wind and dynamical ejecta (e.g. from Wollaeger et al. 2017). To match the broad UV emission, Evans et al. (2017) required a large amount of high- Y_e wind ejecta ($\sim 0.01 - 0.03 M_{\odot}$), with a relatively low amount of low- Y_e dynamical ejecta ($\sim 0.002 - 0.01 M_{\odot}$). The analysis of Cowperthwaite et al. (2017) argued for a total ejecta mass of $0.04 M_{\odot}$ with 1% of this mass in lanthanides. In this paper, we assume a range of ejecta masses ($0.01 - 0.04 M_{\odot}$) and compositions (Tanvir et al. 2017; Evans et al. 2017; Troja et al. 2017).

In Table 1, we convolve the ejecta mass ranges inferred from GW170817 with the observed or calculated mass fractions of different elements or groups of isotopes. The second column ($M_{\text{ejected}}^{\text{obs}}$) lists masses computed assuming the observed solar r-process residuals, while the third column ($M_{\text{ejected}}^{\text{w/nuc.}}$) lists the ranges computed theoretically from first principles (see Section 2.2). The former is de-

TABLE 1
YIELDS OF THE R-PROCESS CONSTITUENTS AS INFERRED FROM GW170817 (EVANS ET AL. 2017; TANVIR ET AL. 2017; TROJA ET AL. 2017). SECOND COLUMN: USING OBSERVED SOLAR R-PROCESS RESIDUALS. THIRD COLUMN: USING THEORETICAL NUCLEOSYNTHETIC YIELDS. A AND Z REPRESENT THE MASS AND ATOMIC NUMBERS, RESPECTIVELY.

Abundance	$M_{\text{ejected}}^{\text{obs}} [M_{\odot}]$	$M_{\text{ejected}}^{\text{w/nuc.}} [M_{\odot}]$
Total r-process ($A > 80$)	$0.01 - 0.03$	$0.008 - 0.055$
Main r-process ($A > 130$)	$0.008 - 0.028$	$0.006 - 0.05$
1st peak ($30 < Z < 38$)	$0.004 - 0.012$	$0.001 - 0.04$
2nd peak ($48 < Z < 59$)	$0.005 - 0.016$	$0.003 - 0.04$
3rd peak ($74 < Z < 82$)	$0.0008 - 0.004$	$0.0004 - 0.02$
Trans-lead ($Z > 82$)	$0.0002 - 0.001$	$0.00002 - 0.008$
Iron Peak ($21 < Z < 30$)	$(5 - 14) \times 10^{-6}$	$(5 - 14) \times 10^{-6}$
Europium	$(3 - 15) \times 10^{-6}$	$(0.5 - 25) \times 10^{-6}$
^{56}Ni	0.0	0.0

signed to test the hypothesis that GW170817 is a typical, representative event which produces a regular r-process signature, consistent with the robust abundance pattern observed in metal-poor halo stars (Sneden et al. 2008) and the ultra-faint dwarf galaxy Reticulum II (Ji et al. 2016). This case is studied in Section 4.1. If the masses of the two neutron stars are different (as suggested by the gravitational wave observation), the observed mass may be greater than typical NS-NS mergers.

2.2. Uncertainties from Nuclear Physics

The consistency between the r-process pattern observed in metal-poor halo stars (Sneden et al. 2008), the solar r-process residuals (Arnould et al. 2007), and the ultra-faint dwarf galaxy Reticulum II (Ji et al. 2016) places tight constraints on the site of the main r-process. To agree with observations, a feasible candidate needs to be able to reproduce the observed pattern robustly, with little sensitivity to the variations in system parameters (Korobkin et al. 2012). However, the current nuclear theory of heavy element nucleosynthesis produces uncertainties in the predicted pattern exceeding observational constraints by at least one order of magnitude (Mumpower et al. 2016b). For this reason, we explore two approaches: one in which the observed solar abundance distribution is assumed, and one in which we simulate the nucleosynthesis from first principles.

The nuclear physics uncertainties mainly stem from the fact that the r-process path meanders through the uncharted territory of heavy, extremely neutron-rich nuclei close to the neutron drip line, for which no experimental data is available. Variations in the unknown nuclear masses, fission fragment distribution, neutron capture rates, β -decay rates, and the specifics of the fission mechanism itself can all significantly impact nucleosynthetic yields (Mumpower et al. 2016b).

We calculate abundance yields with a variety of nuclear mass models and fission fragment distributions. We use nuclear reactions (Mumpower et al. 2016a) and decay models (Mumpower et al. 2016b) which are updated self-consistently with nuclear masses as in Mumpower et al. (2015). The β -delayed and neutron-induced fission rates used were calculated within this same self-consistent framework. The bands in Figure 1 demonstrate the wide range of abundance predictions when the

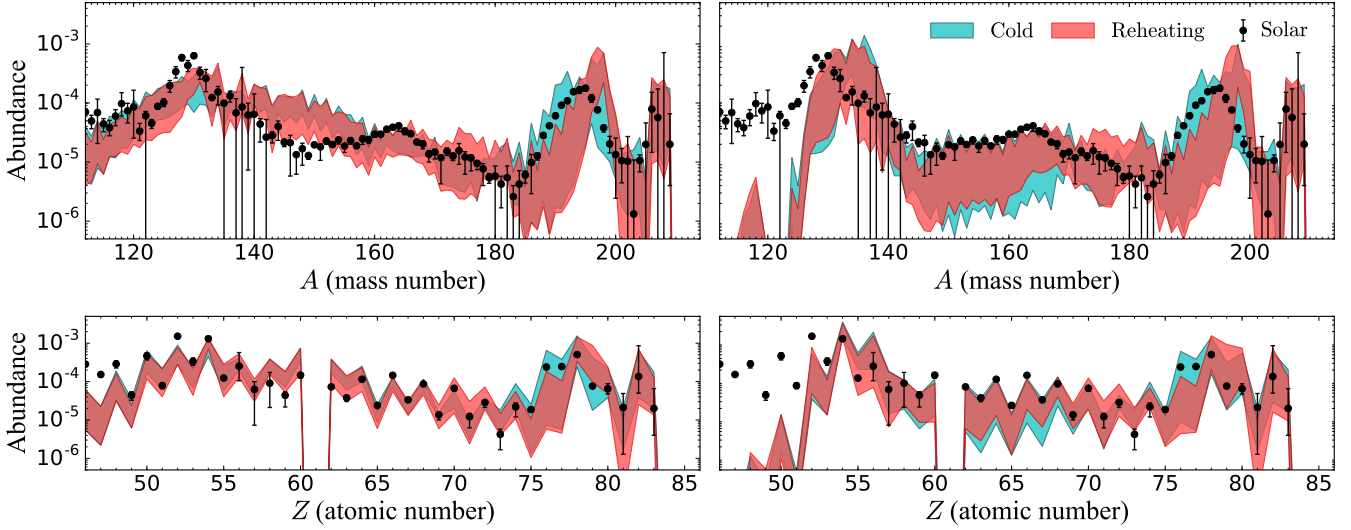


FIG. 1.— The range in the calculated r-process abundance as a function of mass number A (upper row) and atomic number Z (lower row) generated from a set of ten different mass models (DZ, FRDM1995, FRDM2012, HFB17, HFB21, HFB24, WS3, KUY, SLY4, and UNEDF0), assuming Kodama & Takahashi (1975) (left panels) and a symmetric split (right panels) for the fission fragment distribution. Turquoise bands represent very neutron rich, cold merger outflow conditions (Just et al. 2015) without reheating while red bands represent conditions for “slow” ejecta (Mendoza-Temis et al. 2015) with reheating included. The dots are the observed solar r-process residuals (taken from Arnould et al. 2007).

fission fragment distribution is fixed and different mass models are considered. Even more striking in Figure 1 is the difference in the predictions using different fission fragment distributions.

For GW170817, the constraints on the 2nd and 3rd peak r-process yields are set by the amount of high-opacity lanthanide elements needed to explain the late-time “red” kilonova emission. Uncertainties in the nuclear cross-sections can produce the same total lanthanide ejecta, but vary the production of individual components wildly. Keeping the amount of total lanthanides equal (their mass is constrained by the observations), we can study the additional uncertainty in the trans-lead, Eu, and r-process peak elements. The final column of Table 1 shows the yield range including the nuclear physics uncertainties outlined in Table 2 which are based on the range of abundance predictions given by the nuclear mass models and fission fragment distributions considered (outlined in Figure 1). In this range of models, we find that the total Eu abundance can increase or decrease by a factor of 2 with the same total lanthanide abundance.

3. MERGER RATE DENSITIES

Here we briefly describe our methodology to connect our results to LIGO/Virgo’s measurement. More details can be found in C17a.

3.1. Population Synthesis

Population synthesis models predict NS-NS merger rates for individual stellar populations (e.g., Fryer et al. 1999; Voss & Tauris 2003; Mennekens & Vanbeveren 2014; Dominik et al. 2012; Belczynski et al. 2016a; Chruslinska et al. 2017). Those models can be confronted with the observed merger rate estimated from several known NS-NS systems in the Milky Way (21^{+28}_{-14} Myr $^{-1}$, Kim et al. 2015). For comparison with other observational constraints such as short-duration gamma-

ray bursts (Berger 2014) and gravitational wave measurements (Abbott et al. 2016), a calculation of cosmological NS-NS merger rate densities is required. This involves tracing the formation of NS-NS progenitor systems according to the cosmic star formation history (CSFH, Madau & Dickinson 2014) and following their evolution until they merge using metallicity-dependent delay-time distributions (DTDs, see Belczynski et al. 2016b).

The merger rate densities based on previous calculations (Belczynski et al. 2016a) are too low compared to the latest LIGO/Virgo’s estimates at low redshift⁹ ($\sim 1540^{+3200}_{-1220}$ Gpc $^{-3}$ yr $^{-1}$, Abbott et al. 2017). Those models have been revisited by Chruslinska et al. (2017). For many realizations of the input physics, the classical evolution of isolated binaries typically leads to low merger rate densities at low redshifts ($\lesssim 50$ Gpc $^{-3}$ yr $^{-1}$). However, several models with specific common envelope physics, low angular momentum loss during Roche-lobe overflow, electron-capture SNe allowed in a wide range of initial stellar masses (with no natal kick applied), and reduced natal kicks for NS progenitors with heavily stripped envelopes, can produce local NS-NS merger rate densities as high as $\sim 500 - 600$ Gpc $^{-3}$ yr $^{-1}$.

Uncertainties associated with the CSFH, the stellar initial mass function, the binary fraction, and the evolution of metallicity through cosmic time can further shift the predicted merger rate densities by a factor of ~ 2 . The highest merger rate density predicted with the calculations of Chruslinska et al. (2017) is shown as the upper limit of the green shaded area in Figure 2. This limit ($\sim 10^3$ Gpc $^{-3}$ yr $^{-1}$ at redshift $z = 0$) represents the most optimistic model increased by a factor of 2 to show the currently attainable maximum NS-NS merger rate density with population synthesis methods. The lower limit is the same as in C17a (but see Chruslinska et al. 2017).

⁹ As a point of reference, NGC 4993, the host galaxy of GW170817, is at 40 Mpc ($z \sim 0.01$).

TABLE 2
THE MASS FRACTION RANGE FOR ^{151}Eu , ^{153}Eu , AS WELL AS THE RELATIVE ABUNDANCE RANGE $(Y_{\text{max}} - Y_{\text{min}})/\bar{Y}$ FOR ALL STABLE EUROPIUM ISOTOPES. Y_{max} , Y_{min} , AND \bar{Y} ARE THE MAXIMUM, MINIMUM, AND MEAN EUROPIUM r -PROCESS ABUNDANCE, RESPECTIVELY, CALCULATED WITH THE SET OF TEN MASS MODELS OUTLINED IN FIGURE 1 (SEE SECTION 2.2).

Astrophysical Trajectory	Fission Fragment Distribution	^{151}Eu Mass Fraction [10^{-3}]	^{153}Eu Mass Fraction [10^{-3}]	Relative Abundance Range
Cold outflow (no reheating) (Just et al. 2015)	Kodama & Takahashi (1975) Symmetric Split	(5.01 – 11.7) (0.083 – 2.65)	(3.92 – 8.75) (0.12 – 2.84)	0.776 3.239
“Slow” ejecta with reheating (Mendoza-Temis et al. 2015)	Kodama & Takahashi (1975) Symmetric Split	(2.67 – 13.3) (0.19 – 2.09)	(1.89 – 9.62) (0.24 – 2.23)	1.568 2.755

The merger rate density peaks at $z \sim 1.5$ and is shifted compared to the CSFH peak ($z \sim 2$) because of the functional form and metallicity-dependence of the DTD of NS-NS mergers.

3.2. Galactic Chemical Evolution

To calculate the merger rate densities required by GCE, we use the same convolution process with the CSFH as in Section 3.1. However, instead of using the NS-NS merger rates predicted by population synthesis for individual stellar populations, we use the ones adopted in GCE simulations. Those rates are calibrated to reproduce the $[\text{Eu}/\text{Fe}]^{10}$ abundances observed in the Milky Way, assuming NS-NS mergers are the only source of r-process elements.

The merger rate density required to reproduce the $[\text{Eu}/\text{Fe}]$ abundance pattern depends on the DTD of NS-NS mergers, on the chemical evolution code, and on the amount of Eu and Fe ejected by NS-NS mergers and supernovae, respectively. The range of solutions for a DTD in the form of t^{-1} is shown as the dark and light blue shaded areas in Figure 2 (see Section 4 for details).

4. THE R-PROCESS IN THE MILKY WAY

There is a degeneracy between the rate required by GCE and the average mass of Eu ejected by NS-NS mergers. For example, if NS-NS mergers release less r-process material, more mergers will be needed to recover the same level of enrichment. The two blue dashed lines in Figure 2 show the merger rate densities required by GCE when the average Eu yields are $3 \times 10^{-6} M_{\odot}$ and $1.5 \times 10^{-5} M_{\odot}$, representing the lower and upper limits derived for GW170817 (Section 2) when assuming a typical r-process abundance pattern for the ejecta.

The dark blue shaded area surrounding these two lines represents the uncertainties caused by using different Fe yields for massive stars and by using different GCE studies to infer the required merger rate (see C17a). If we use theoretical calculations from first principles to calculate the abundance pattern of the ejecta, the range of Eu yields for GW170817 becomes significantly larger because of nuclear astrophysics uncertainties (see Section 2.2), which reduces our ability to constrain the contribution of NS-NS mergers using GCE arguments (lighter blue shaded area in Figure 2).

Overall, there is an overlap between GCE, population synthesis, and LIGO/Virgo between ~ 300 and

¹⁰ $[\text{A}/\text{B}] = \log_{10}(n_A/n_B) - \log_{10}(n_A/n_B)_{\odot}$ where n_A and n_B are the number densities of elements A and B. This elemental ratio is normalized to the solar value.

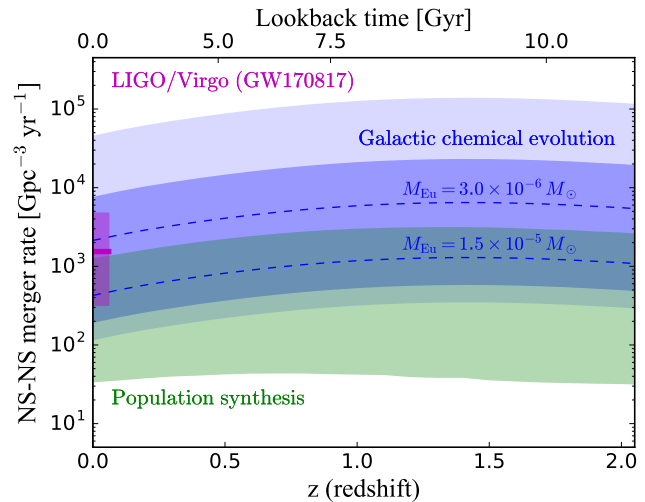


FIG. 2.— Neutron star - neutron star (NS-NS) merger rate density as a function of redshift. The two blue dashed lines show the specific rates needed in galactic chemical evolution (GCE) studies to reproduce the amount of Eu observed in the Milky Way, when each NS-NS merger is assumed to eject on average $3 \times 10^{-6} M_{\odot}$ and $1.5 \times 10^{-5} M_{\odot}$ of Eu. These values represent the lower and upper limits of the total ejecta mass derived for GW170817 (Section 2), when assuming a typical r-process abundance pattern for the ejecta. The dark blue shaded area shows the range of rates associated with those two values when GCE uncertainties are considered (see Section 4 for more details). The lighter (and larger) blue shaded area shows the range required when Eu yields are calculated theoretically from first principles, accounting for nuclear physics uncertainties (Section 2.2). The green shaded area represents the rates predicted using the population synthesis models of Belczynski et al. (2016a) and Chruslinska et al. (2017). The pink thick horizontal line and shaded area show the local rate and uncertainty provided by LIGO/Virgo from GW170817 (Abbott et al. 2017).

$\sim 1000 \text{ Gpc}^{-3} \text{ yr}^{-1}$. GCE and population synthesis are consistent with each other if NS-NS mergers eject on average $\gtrsim 10^{-5} M_{\odot}$ of Eu.

4.1. If GW170817 is a Representative Event

The NS-NS merger rate densities derived from GW170817 (pink shaded area in Figure 2) are remarkably consistent with the GCE requirement if a typical r-process pattern is assumed for its ejecta (dark blue shaded area). If GW170817 is statically a representative event, this detection suggests that NS-NS mergers are likely to be the main r-process site in the Milky Way and possibly in other galaxies.

Using the one-zone GCE code OMEGA (Côté et al. 2017b), we calculate a current Galactic merger rate of ~ 50 and $\sim 230 \text{ Myr}^{-1}$ for Eu yields of 1.5×10^{-5} and

$3 \times 10^{-6} M_{\odot}$, respectively. The final ($z = 0$) star formation rate in our Milky Way model is $2.5 M_{\odot} \text{ yr}^{-1}$. Accounting for uncertainties in this final rate, which observationally ranges from 0.65 to $3 M_{\odot} \text{ yr}^{-1}$ (e.g., Kubryk et al. 2015), and in the Fe yields used in GCE studies (see Figure 1 in C17a), we obtain NS-NS merger rates in the range of [5 – 100] and [35 – 495] Myr^{-1} for the upper and lower Eu yields limits, respectively. Those ranges are within the [1 – 1000] Myr^{-1} range estimated by Abadie et al. (2010) from pulsar luminosities but are wider than the [7 – 49] Myr^{-1} range derived by Kim et al. (2015). However, Chruslinska et al. (2017) suggested that the range provided by Kim et al. (2015) could be extended to [2 – 210] Myr^{-1} if uncertainties in the pulsar luminosity function were included (see their Section 5.1).

The GCE requirement overlaps and is consistent with both the cosmic merger rate density in $\text{Gpc}^{-3} \text{ yr}^{-1}$ and the Galactic merger rate in Myr^{-1} . In particular, our Galactic merger rates are in better agreement with Kim et al. (2015) when the assumed Eu yields are $\gtrsim 10^{-5} M_{\odot}$, which turns out to be the regime where GCE, population synthesis, and LIGO/Virgo are overlapping.

4.2. If GW170817 is Not a Representative Event

So far, only one NS-NS has been detected by LIGO/Virgo, which means that GW170817 could be an unusual and non-representative event. Alternatively, the merger rate density could actually be lower, meaning that GW170817 has been detected earlier than statistically expected. If this is the case, the derived NS-NS merger rate will decrease as the LIGO/Virgo's observing time gets longer. However, given the uncertainties, NS-NS mergers could still be the main r-process site even if the merger rate density was reduced, as long as it does not drop below $\sim 100 – 200 \text{ Gpc}^{-3} \text{ yr}^{-1}$. On the other hand, if GW170817 has been detected later than statistically expected, the actual merger rate density could be higher.

GW170817 could also be unusual in terms of its mass ejected. If NS-NS mergers eject on average more or less mass than GW170817, the range of merger rate densities required by GCE would be shifted downward or upward. Indeed, depending on the masses and mass ratio of the two neutron stars in the merger, the dynamical and wind ejecta masses can vary by a factor of 2 – 4 (Korobkin et al. 2012). The observed masses are uncertain, the inferred neutron star mass ratios range from 0.4 to 1.0 (Abbott et al. 2017). If the mass ratio is closer to 0.4, the ejected mass may be higher than representative values.

5. CONCLUSIONS

We addressed the implication of the first NS-NS merger detected by LIGO/Virgo (GW170817) on the origin of r-process elements. Using the ejected yields estimated for GW170817 (see Table 1), the range of merger rate densities of $320 – 4740 \text{ Gpc}^{-3} \text{ yr}^{-1}$ derived by LIGO/Virgo is consistent with the range required by galactic chemical evolution (GCE) studies to explain the europium (Eu) abundances observed in the Milky Way with NS-NS mergers.

If GW170817 is a representative event and has a typical r-process signature, this new gravitational wave detection supports the theory that NS-NS mergers are the dominant source of r-process elements (see Figure 2). In fact, if NS-NS mergers eject on average $\sim 10^{-5} M_{\odot}$ of Eu, there is an overlap between GCE, population synthesis, Galactic merger rates, and LIGO/Virgo. In case GW170817 is an unusual event, the actual merger rate and typical ejecta mass could be different. But even if the merger rate density is reduced to $\sim 100 – 200 \text{ Gpc}^{-3} \text{ yr}^{-1}$, NS-NS mergers could still be the dominant r-process site, as long as the typical Eu yields stay larger than $\sim 10^{-5} M_{\odot}$.

If astrophysical simulations are used instead of assuming a typical r-process pattern to derive the Eu yields for GW170817, we found that uncertainties in nuclear masses and fission properties need to be reduced in order to better constrain the role of NS-NS mergers on the chemical evolution of r-process elements using LIGO/Virgo's detections. In any event, it is clear that significant advancements in our knowledge of the properties of nuclei far from stability are required to understand NS-NS merger nucleosynthesis from first principles.

ACKNOWLEDGEMENTS

This research is supported by the National Science Foundation (USA) under grant No. PHY-1430152 (JINA Center for the Evolution of the Elements) and by the ERC Consolidator Grant (Hungary) funding scheme (project RADIOSTAR, G.A. n. 724560). K.B. acknowledges support from the NCN grants Sonata Bis 2 (DEC-2012/07/E/ST9/01360), OPUS (2015/19/B/ST9/01099) and OPUS (2015/19/B/ST9/03188). N.V. and R.S. are supported by the U.S. Department of Energy under Contract No. DE-AC52-07NA27344 for the topical collaboration Fission In R-process Elements (FIRE). This work was also supported in part by the U.S. Department of Energy under grant number DE-SC0013039 (R.S. and T.S.). A portion of this work was also carried out under the auspices of the National Nuclear Security Administration of the U.S. Department of Energy at Los Alamos National Laboratory under Contract No. DE-AC52-06NA25396 (C.F., O.K., R.W., M.M.). This research used resources provided by the Los Alamos National Laboratory Institutional Computing Program (O.K., R.W.).

REFERENCES

Abadie, J., Abbott, B. P., Abbott, R., et al. 2010, *Classical and Quantum Gravity*, 27, 173001
 Abbott, B. P., Abbott, R., Abbott, T. D., et al. 2016, *ApJ*, 832, L21
 Abbott, B. P., LIGO Scientific Collaboration and Virgo Collaboration 2017, *Physical Review Letters*, 119, 161101
 Arnould, M., Goriely, S., & Takahashi, K. 2007, *Phys. Rep.*, 450, 97
 Belczynski, K., Holz, D. E., Bulik, T., & O'Shaughnessy, R. 2016a, *Nature*, 534, 512
 Belczynski, K., Repetto, S., Holz, D. E., et al. 2016b, *ApJ*, 819, 108

Berger, E. 2014, *ARA&A*, 52, 43

Bovard, L., Martin, D., Guercilena, F., et al. 2017, ArXiv e-prints, [arXiv:1709.09630](https://arxiv.org/abs/1709.09630)

Burris, D. L., Pilachowski, C. A., Armandroff, T. E., et al. 2000, *ApJ*, 544, 302

Cescutti, G., Romano, D., Matteucci, F., Chiappini, C., & Hirschi, R. 2015, *A&A*, 577, A139

Chruslinska, M., Belczynski, K., Klencki, J., & Benacquista, M. 2017, ArXiv e-prints, [arXiv:1708.07885](https://arxiv.org/abs/1708.07885)

Cowperthwaite, P. S., Berger, E., Villar, V. A., et al. 2017, *ApJ*, 848, L17

Côté, B., Belczynski, K., Fryer, C. L., et al. 2017a, *ApJ*, 836, 230

Côté, B., O’Shea, B. W., Ritter, C., Herwig, F., & Venn, K. A. 2017b, *ApJ*, 835, 128

Dietrich, T., & Ujevic, M. 2017, *Classical and Quantum Gravity*, 34, 105014

Dominik, M., Belczynski, K., Fryer, C., et al. 2012, *ApJ*, 759, 52

Evans, P. A., Cenko, S. B., Kennea, J. A., et al. 2017, *Science*, doi:10.1126/9580

Fryer, C. L., Woosley, S. E., & Hartmann, D. H. 1999, *ApJ*, 526, 152

Hotokezaka, K., Kiuchi, K., Kyutoku, K., et al. 2013, *Phys. Rev. D*, 87, 024001

Ji, A. P., Frebel, A., Chiti, A., & Simon, J. D. 2016, *Nature*, 531, 610

Jin, Z.-P., Li, X., Cano, Z., et al. 2015, *ApJ*, 811, L22

Just, O., Bauswein, A., Pulpillo, R. A., Goriely, S., & Janka, H. T. 2015, *MNRAS*, 448, 541

Kasliwal, M. M., Korobkin, O., Lau, R. M., Wollaeger, R., & Fryer, C. L. 2017, *ApJ*, 843, L34

Kim, C., Perera, B. B. P., & McLaughlin, M. A. 2015, *MNRAS*, 448, 928

Kodama, T., & Takahashi, K. 1975, *Nuclear Physics A*, 239, 489

Korobkin, O., Rosswog, S., Arcones, A., & Winteler, C. 2012, *MNRAS*, 426, 1940

Kubryk, M., Prantzos, N., & Athanassoula, E. 2015, *A&A*, 580, A126

Lattimer, J. M., & Schramm, D. N. 1974, *ApJ*, 192, L145

Lippuner, J., Fernández, R., Roberts, L. F., et al. 2017, *MNRAS*, 472, 904

Lippuner, J., & Roberts, L. F. 2015, *ApJ*, 815, 82

Madau, P., & Dickinson, M. 2014, *ARA&A*, 52, 415

Matteucci, F., Romano, D., Arcones, A., Korobkin, O., & Rosswog, S. 2014, *MNRAS*, 438, 2177

Mendoza-Temis, J. J., Wu, M. R., Langanke, K., et al. 2015, *Phys. Rev. C*, 92, 055805

Mennekens, N., & Vanbeveren, D. 2014, *A&A*, 564, A134

Mumpower, M. R., Kawano, T., & Möller, P. 2016a, *Phys. Rev. C*, 94, 064317

Mumpower, M. R., Surman, R., Fang, D.-L., et al. 2015, *Phys. Rev. C*, 92, 035807

Mumpower, M. R., Surman, R., McLaughlin, G. C., & Aprahamian, A. 2016b, *Progress in Particle and Nuclear Physics*, 86, 86

Nishimura, N., Takiwaki, T., & Thielemann, F.-K. 2015, *ApJ*, 810, 109

Rosswog, S. 2013, *Philosophical Transactions of the Royal Society of London Series A*, 371, 20120272

Sneden, C., Cowan, J. J., & Gallino, R. 2008, *ARA&A*, 46, 241

Tanvir, N. R., Levan, A. J., Fruchter, A. S., et al. 2013, *Nature*, 500, 547

Tanvir, N. R., Levan, A. J., Gonzalez-Fernandez, C., et al. 2017, *ApJ*, 848, L27

Thielemann, K. F., Eichler, M., Panov, I. V., & Wehmeyer, B. 2017, *Annual Review of Nuclear and Particle Science*, 67, annurev

Troja, E., Piro, L., van Eerten, H., et al. 2017, *Nature*, doi:10.1038/24290

Voss, R., & Tauris, T. M. 2003, *MNRAS*, 342, 1169

Wehmeyer, B., Pignatari, M., & Thielemann, F.-K. 2015, *MNRAS*, 452, 1970

Wollaeger, R. T., Korobkin, O., Fontes, C. J., et al. 2017a, ArXiv e-prints, [arXiv:1705.07084](https://arxiv.org/abs/1705.07084)

Yang, B., Jin, Z.-P., Li, X., et al. 2015, *Nature Communications*, 6, 7323